Konrad-Zuse-Zentrum für Informationstechnik Berlin

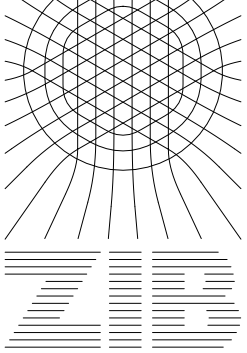

J. Ackermann B. Erdmann R. Roitzsch

A Self–Adaptive Multilevel Finite Element Method for the Stationary Schrödinger Equation in Three Space Dimensions

Preprint SC 94–10 (May 1994)

A Self–Adaptive Multilevel Finite Element Method for the Stationary Schrödinger Equation in Three Space Dimensions

J. Ackermann, B. Erdmann and R. Roitzsch
Konrad-Zuse-Zentrum Berlin (ZIB), Heilbronner Str. 10,
10711 Berlin, Germany

Abstract An error controlled finite elemente method (FEM) for solving stationary Schrödinger equations in three space dimensions is proposed. The method is based on an adaptive space discretization into tetrahedra and local polynomial basis functions of order $p = 1$–5 defined on these tetrahedra. According to a local error estimator the triangulation is automatically adapted to the solution. Numerical results for standard problems appearing in vibrational motion and molecular structure calculations are presented and discussed. Relative precisions better than 1e-8 are obtained. For equilateral H_3^{++} the adaptive FEM turns out to be superior to global basis set expansions in the literature. Our precise FEM results exclude in a definite manner the stability or metastability of equilateral H_3^{++} in its groundstate.

1. Introduction

The finite element method (FEM) [1–2] in one and two space dimensions has been reported as a very efficient tool for the treatment of atoms and diatomic molecules [4–16]. Due to the local approximation properties of the FEM there exists a reasonable interest to use it in multi–nuclear molecular structure calculations too.

The essential requirement for the application of the FEM to multi-atom systems is the extension to arbitrary potentials in three space dimensions. Since, however, for arbitrary geometrical configurations of the nuclear centers any symmetry property will be lost, there will be no chance to find special coordinate systems, similar to those, which have been found favorable in the diatomic case. Using instead cartesian coordinates the FEM has to deal with highly peaked wavefunctions and thus an appropriate fine space discretization will be needed to resolve them. A properly fine uniform 3D mesh would lead to a computational amount of work, which is beyond the feasibility of modern supercomputers. However, a sophisticated reduction of the computational work is possible with the concept of adaptivity. The applicability of this concept to 2D stationary Schrödinger eigenvalue problems, including accurate treatments for H_2^+ and linear H_3^{2+}, is demonstrated in [17, 18]. In the present work an extension to 3D problems is proposed.

The wavefunction is approximated by a space discretization into tetrahedra and the linear combination of local polynomial functions defined on these tetrahedra. The FEM approximation is improved through a step by step refinement of the 3D mesh. An estimator for the local approximation errors selects the relevant tetrahedra to be refined. In this way the 3D mesh is adapted to the solution.

Section 2 is devoted to the description of the multilevel method, including the FEM discretization, the local polynomials being used, the solution of the matrix eigenvalue problems, the error estimator, the local refinement and a short comment on the expected convergence behavior of the method. In section 3 we give numerical results for different 3D Schrödinger equations; the vibrational motion of a mass in a non–isotropic harmonic potential, the two–center one–electron problem (H_2^+ molecule) in cartesian coordinates and the three–center one–electron problem in the equilateral triangle geometry (equilateral H_3^{2+}) serve as examples to test the adaptive FEM.

2. Outline of the method

We consider the stationary Schrödinger–equation

$$(\mathcal{H} - E)\Psi = 0 \quad \text{on} \quad \Omega \subset \mathbb{R}^3 \tag{1}$$

where $E \in \sigma(\mathcal{H})$ denotes a discrete eigenvalue of the quantum Hamiltonian $\mathcal{H}$. Using the Ansatz

$$\Psi \approx \tilde{\Psi} = \sum_{i=1}^{M} C_i \phi_i \qquad . \tag{2}$$

and applying the variational principle yields the general matrix eigenvalue problem:

$$(\mathbf{H} - \tilde{E}\ \mathbf{S})\mathbf{C} = 0 \qquad . \tag{3}$$

The elements of the Hamiltonian matrix $\mathbf{H}$ and the overlap matrix $\mathbf{S}$ are given by

$$H_{ij} = \langle \phi_i, \mathcal{H}\phi_j \rangle := \int_\Omega \phi_i (\mathcal{H}\phi_j)\ d\Omega \tag{4}$$

$$S_{ij} = \langle \phi_i, \phi_j \rangle := \int_\Omega \phi_i \phi_j\ d\Omega \quad . \tag{5}$$

Solving (3) leads to the unknown coefficients $\mathbf{C} = (C_i)$ in (2) and an upper bound for the eigenvalue E

$$\tilde{E} \geq E \quad . \tag{6}$$

In this work we use a continuous piecewise polynomial approximation of Ψ, known as finite element discretization. Therefore the domain Ω is segmented into three–dimensional (3D) tetrahedra. On this partition a FEM basis $\{\phi_i, i = 1, 2, \ldots, M\}$ of local functions, continuous on Ω and polynomial on each tetrahedron, is defined.

A finite element method, in which the triangulation is fixed and the polynomial degree p of the local functions is increased in order to reduce the approximation error, is called a p–version. An alternative method is the h–version FEM, where the polynomial degree

is fixed (usual $p = 1$) and the mesh size h is reduced to obtain the desired accuracy. We consider a multilevel adaptive mesh refinement (h–version) in combination with a moderate (global) variation of the polynomial approximation order from $p = 1$ up to $p = 5$. The flow diagram of this multilevel h–adaptive FEM is plotted in figure 1.

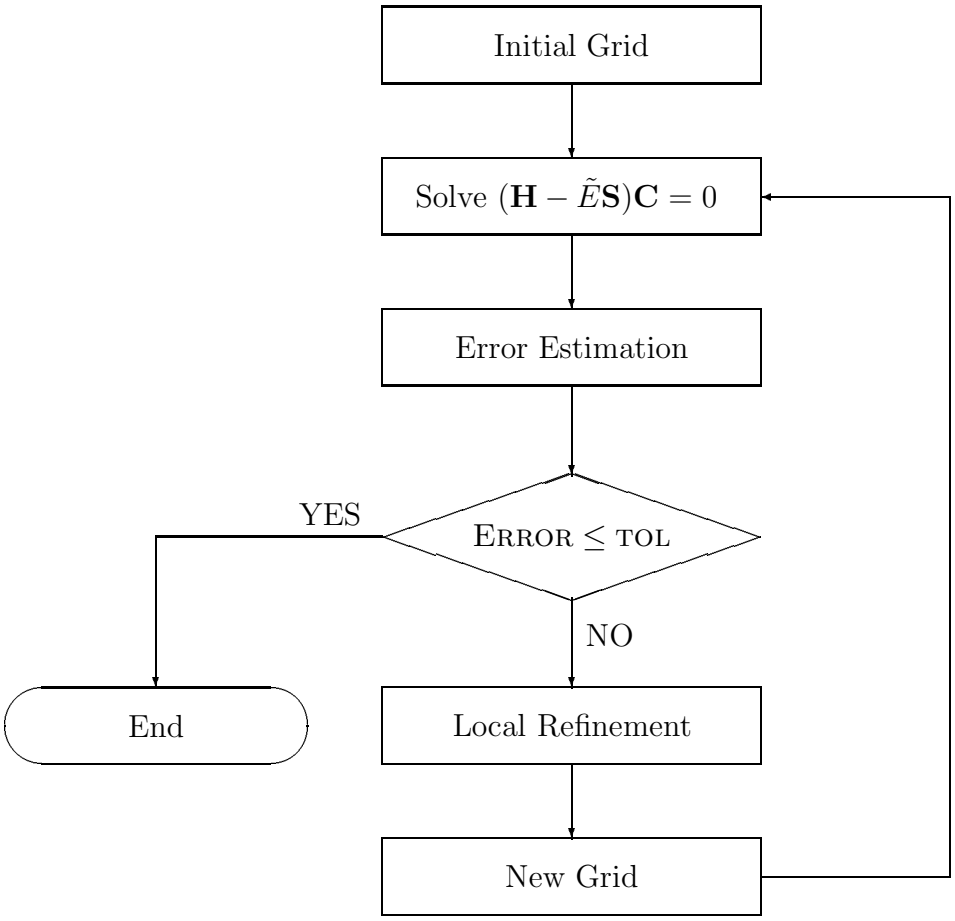

Figure 1: Flow diagram of the adaptive refinement.

We start with an initial, in general very coarse grid and compute the FEM approximation $\tilde{\Psi}$ for a given polynomial order p, by assembling and solving the corresponding general matrix eigenvalue equation (3). Now the local error estimator indicates which of the tetrahedra must be refined to improve the approximation of Ψ, and the adaptive local refinement of these tetrahedra leads to a new grid. Computing the FEM approximation $\tilde{\Psi}$ on the refined grid, error estimation and local refinement are now repeated iteratively to construct a grading in the triangulation adapted to the exact wavefunction. The iterative process is stopped when the estimated global error reaches the desired accuracy TOL. In the field of elliptic boundary value problems involving partial differential equations, such adaptive techniques have been standard for many

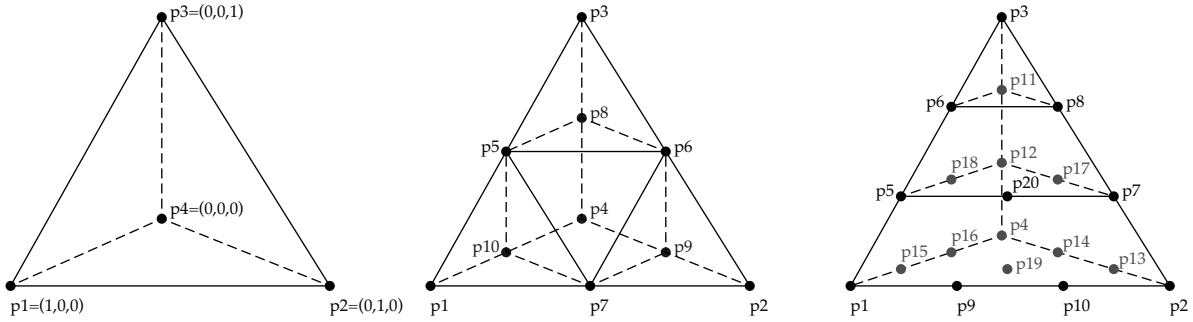

Figure 2 : Nodes on the reference tetrahedron for linear, quadratic and cubic shape functions.

years. Software packages like KASKADE [19, 20] or PLTMG [21] are based on this concept. We use the KASKADE software toolbox to implement an adaptive FEM for Schrödinger eigenvalue problems. In the following we will describe each of the steps in figure 1 in more detail.

First we define the local basis functions used in our FEM. From the very beginning it was clear that the standard linear shape functions were unsuitable to achieve high accurate results [17]. Thus we additionally implemented higher order ($p = 2 - 5$) polynomials of the Lagrange type [3]. It is sufficient to construct these local polynomials for a reference tetrahedron with corner points $p_1 = (1, 0, 0)$, $p_2 = (0, 1, 0)$, $p_3 = (0, 0, 1)$, $p_4 = (0, 0, 0)$, as shown in figure 2. Then shape functions for an arbitrary tetrahedron are given via an affine variable transformation [2]. It is convenient to use volume coordinates

$$L_1 = 1 - x - y - z, \quad L_2 = x, \quad L_3 = y, \quad L_4 = z, \tag{7}$$

instead of the cartesian coordinates x, y, z. First, for a given p we define $p+1$ equidistant points $\{\xi_i = i/p, i = 0, 1, \ldots, p\}$ on the interval $[0, 1]$. Appropriate polynomials in one volume coordinate are

$$l_I^I(L_k) := \frac{(L_k - \xi_0)(L_k - \xi_1) \cdots (L_k - \xi_{I-1})}{(\xi_I - \xi_0)(\xi_I - \xi_1) \cdots (\xi_I - \xi_{I-1})} \qquad 0 < I \leq p \tag{8}$$

and $l_0^0(L_k) := 1$. These polynomials giving unity at one point $L_k = \xi_I$ and passing through I points $L_k = \xi_i$, $i = 0, 1, \ldots, I-1$ are known as Lagrange polynomials. For every quadruplet of integers (I, J, K, L) with $I + J + K + L = p$ we get one of the desired shape functions φ_i by the product of Lagrange polynomials :

$$\varphi_i = l_I^I(L_1) l_J^J(L_2) l_K^K(L_3) l_L^L(L_4) \qquad . \tag{9}$$

A family of such functions φ_i with $I+J+K+L = p$ builds a complete set of polynomials of order p in $\mathbb{R}^3$. For linear elements ($p = 1$) we simply get $\xi_0 = 0, \xi_1 = 1$ and with

$I + J + K + L = 1$:

$$\begin{aligned} \varphi_1 &= x \\ \varphi_2 &= y \\ \varphi_3 &= z \\ \varphi_4 &= L_1 = 1 - x - y - z \quad . \end{aligned}$$

It is easy to verify that

$$\varphi_i(p_j) = \delta_{ij} \tag{10}$$

is valid for the corner nodes $p_j, j = 1, 2, 3, 4$ in figure 2a. Points on the tetrahedron satisfying (10) are called nodal points.

The quadratic functions φ_i are given by:

$$\begin{aligned} \varphi_1 &= (2x-1)x & \qquad \varphi_6 &= 4yz \\ \varphi_2 &= (2y-1)y & \varphi_7 &= 4xy \\ \varphi_3 &= (2z-1)z & \varphi_8 &= 4L_1 z \\ \varphi_4 &= (2L_1-1)L_1 & \varphi_9 &= 4L_1 y \\ \varphi_5 &= 4xz & \varphi_{10} &= 4L_1 x \quad . \end{aligned}$$

An impression of the form of these functions may be got from the distribution of the nodal points on the tetrahedron in figure 2b. The quadratic functions $\varphi_i, i = 1, 2, \ldots, 4$ are associated by (10) to the corner nodes, whereas $\varphi_i, i = 5, 6, \ldots, 10$ are connected to the midpoints of the edges. For the polynomial order $p = 3$ we get one nodal point on each corner, two on each edge and one at each of the midpoints of the faces, see figure 2c. Since the construction of polynomial basis sets for $p > 2$ is straightforward we abstain from listing the 20 cubic, the 35 quartic and the 56 quintic functions.

We now turn to the second step of the multilevel method plotted in figure 1: the general matrix eigenvalue problem (3). For a given grid and polynomial order p the matrix elements (4) of $\mathbf{H}$ and $\mathbf{S}$ are computed by a sufficient accurate Gauss integration formula [22, 23]. To get the FEM approximation $\tilde{\Psi}$ we must solve the general matrix eigenvalue problem (3). In the case of very coarse grids and corresponding small matrix dimensions M this is done by Givens rotation. However, to achieve results of high accuracy, the matrix dimension has to be raised (see section 3) and the Givens rotation becomes too costly. Fortunately the matrices are very sparse; the average number of nonzeros in a row is about 14 for linear elements and increases up to 110 for quintic shape functions. To make use of the sparsity of the matrices the inverse vector iteration is applied to solve (3) for matrix dimensions M greater than 90. The inverse vector iteration leads to a sequence of systems of algebraic equations :

$$(\mathbf{H} - \xi\,\mathbf{S})\;\mathbf{C}_i = \mathbf{S}\;\mathbf{C}_{i-1} \qquad i = 1, 2, \ldots \qquad , \tag{11}$$

where ξ is the expected value for the eigenvalue, known from the previous approximation level. For a refined grid the initial vector $\mathbf{C}_0$ is chosen as the corresponding

eigenvector on the previous grid, interpolated on the additional grid points. If only the polynomial order p is increased on the same grid, the old solution is projected into the new (non–hierarchical) basis to get an optimal starting vector.

The linear system (11) is solved via a Cholesky decomposition of the matrix $(\mathbf{H} - \xi\,\mathbf{S})$. To minimize the matrix fill–in produced by the Cholesky decomposition, the numbering of the basis function is reordered by the reverse Cuthill–McKee method [24], but the fill-in is still proportional to $M \log M$ and the amount of operations for solving the linear system is at least $O(M^{3/2})$. Thus for very high dimensions the linear systems (11) are solved via the iterative conjugate gradient (CG) method. Note that the required precision of the CG solver can be coupled to the convergence of the outer inverse vector iteration, i.e. at the initial step of the inverse vector iteration the linear system (11) must not be solved up to a very high precision. But of course, in order to guarantee the convergence of the inverse vector iteration, the precision of the CG-solver must be increased from each invers vector iteration step to the next.

The next step after assembling and solving the general eigenvalue problem (3) is the estimation of the local discretization error, which is necessary to select the tetrahedra for an effective local grid refinement, and the estimation of the global discretization error used as stopping criteria for the multilevel refinement. We tested several different local error estimators and in the following we describe the estimator we found most effective in numerical examples.

The FEM approximation on a given grid depends on the polynomial order p

$$\tilde{\Psi} = \Psi^{(p)} = \sum_{i=1}^{M} C_i \phi_i^{(p)} \qquad . \tag{12}$$

In terms of the normed exact wavefunction Ψ and the normed FEM approximation $\Psi^{(p)}$ the resulting error in the eigenvalue

$$E^{(p)} := \langle \Psi^{(p)}, \mathcal{H}\Psi^{(p)} \rangle \tag{13}$$

is given by

$$\delta E^{(p)} := E^{(p)} - E = \langle (\Psi^{(p)} + \Psi), (\mathcal{H} - \gamma)(\Psi^{(p)} - \Psi) \rangle \qquad . \tag{14}$$

The real shift parameter γ is arbitrary and can be used to replace the below semi-bounded operator $\mathcal{H}$ by the positiv definite (elliptic) operator $\mathcal{H} - \gamma$ by setting $\gamma \leq E_0 := \sup\{e \in \mathbb{R} \mid e \in \sigma(\mathcal{H})\}$. By defining the local discretization error on each of the $N_\bigtriangledown$ tetrahedra

$$\delta\Psi_i^{(p)} := \begin{cases} \Psi^{(p)} - \Psi & \text{on } \bigtriangledown_i \\ 0 & \text{otherwise} \end{cases} \qquad , \tag{15}$$

where $\bigtriangledown_i$ denotes the volume of the tetrahedron i, (14) can be rewritten in the form

$$\delta E^{(p)} = \sum_{i=1}^{N_\bigtriangledown} \delta E_i^{(p)} \tag{16}$$

with

$$\delta E_i^{(p)} = \langle (\Psi^{(p)} + \Psi), (\mathcal{H} - \gamma)\delta\Psi_i^{(p)} \rangle \qquad . \tag{17}$$

The numbers $\delta E_i^{(p)}$ can be interpreted as the contribution of the local discretization error $\delta\Psi_i^{(p)}$ to the error in the FEM eigenvalue $E^{(p)}$. Thus these numbers indicate on which tetrahedra the local discretization error must be reduced, in a h–method by the refinement of these tetrahedra, to improve the FEM eigenvalue $E^{(p)}$ significantly. But, in contrast to the global error $\delta E^{(p)}$, the local error contributions $\delta E_i^{(p)}$ are not unique and depending on the real shift parameter γ not necessarily positive. If we choose $\gamma = E$ we can transform (17) into

$$\delta E_i^{(p)} = \langle \delta\Psi_i^{(p)}, (\mathcal{H} - E)\delta\Psi_i^{(p)} \rangle + \sum_{j \neq i}^{N_\nabla} \langle \delta\Psi_j^{(p)}, (\mathcal{H} - E)\delta\Psi_i^{(p)} \rangle \qquad . \tag{18}$$

The first term in (18) is the shifted energy norm of $\delta\Psi_i^{(p)}$, dominant and positive for $E = E_0$, whereas the sum over the nondiagonal couplings to other tetrahedra in the second term is zero or at least comparatively small.

Of course, $\delta E^{(p)}$ and $\delta E_i^{(p)}$ can not be computed exactly, because the exact wavefunction Ψ and eigenvalue E are unknown in general. Thus we replace Ψ and E by the (normed) next order approximation available on the same grid, i.e. by $\Psi^{(p+1)}$ and $E^{(p+1)}$:

$$\delta\tilde{E}^{(p)} = \langle (\Psi^{(p)} + \Psi^{(p+1)}), (\mathcal{H} - E^{(p+1)})(\Psi^{(p)} - \Psi^{(p+1)}) \rangle \qquad . \tag{19}$$

This approximated error underestimates the exact error

$$\delta\tilde{E}^{(p)} \leq \delta E^{(p)} \qquad , \tag{20}$$

but becomes nearly identical to the exact error for dense grids, see section 3.

In the FEM the local representation $\Psi_i^{(p)}$ of the wavefunction is given in terms of the Lagrange polynomials defined on a tetrahedron. This representation is continuous, i.e. drops smoothly to zero on the adjacent tetrahedra. The difference of the local FEM representation with polynomial order p and $p+1$ is also continuous in this way. For technical reasons (and to avoid the complex mathematical problem concerning the energy norm of the noncontinuous functions $\delta\Psi_i$) we use the continuous difference $\Psi_i^{(p)} - \Psi_i^{(p+1)}$ to compute the relevant quantities

$$\delta\tilde{E}_i^{(p)} = \mid \langle (\Psi^{(p)} + \Psi^{(p+1)}), (\mathcal{H} - E^{(p+1)})(\Psi_i^{(p)} - \Psi_i^{(p+1)}) \rangle \mid \tag{21}$$

for the refinement strategy. Hence to get the estimates (19) and (21) for the global and local error, respectively, we must compute FEM approximations (at least) for two polynomial orders p and $p+1$. The global error estimation (19) indicates either the FEM solution is sufficiently accurate or must be improved by further local refinements. A more rigorous analysis and justification of the discretization and localization of the defect equation (14) leading to the local error estimates (21) should be possible by the theory of space decomposition [25].

The refinement of the grid has to be done in a way preserving the numerical stability of the FEM approximation. This requirement is strongly connected to the geometrical aspects of the grid. In particular, for each tetrahedron t in the successively generated

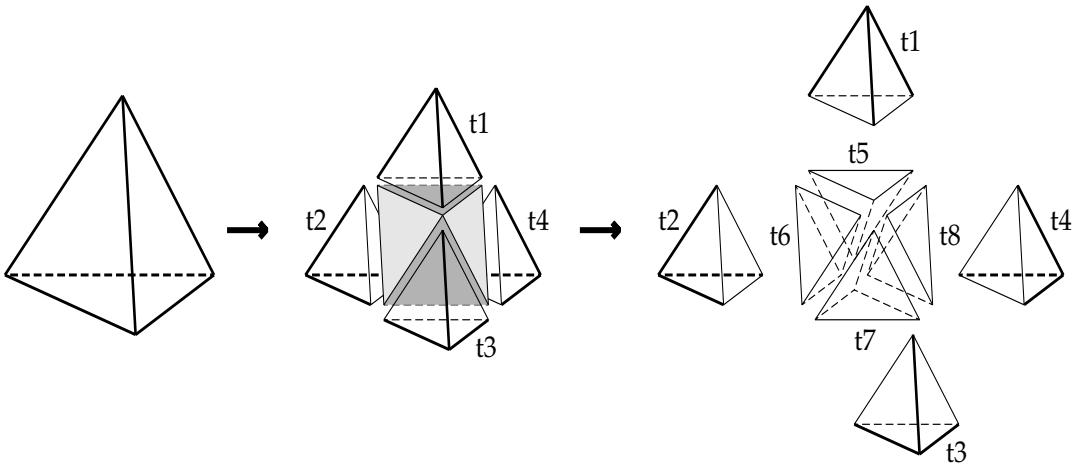

Figure 3 : Regular refinement

triangulations the ratio between the diameters $d_{exterior}$ and $d_{interior}$ of the smallest enveloping (circumscribed) ball and largest interior (inscribed) ball, respectively, should remain uniformly bounded, i.e.

$$d_{exterior}/d_{interior} \leq C \tag{22}$$

holds with a constant C independented of the refinement level for arbitary t. Extensions of the well–known regular (red) 2D–refinements of Bank et al [26] to three dimensions have been considered by various authors [27–30]. By connecting the midpoints of the edges of a tetrahedron t, we obtain four new tetrahedra t_1, t_2, t_3, t_4, each of which corresponds to a vertex of t, and a remaining octahedron, see figure 3. The splitting of the octrahedron in four tetrahedra t_5, t_6, t_7, t_8 is not unique, but depends on the selection of the interior diagonal edge which can be chosen in three ways. Each choice provides a regular (red) refinement of the tetrahedron, but the successive regular refinement may become unstable in the sense of (22), if the diagonal interior edge is not selected properly. However, the authors, mentioned above, developed strategies for stable regular refinement.

After the regular refinement of the tetrahedra selected a non-conforming triangulation results. To obtain a conforming triangulation the transition between refined and non-refined tetrahedra must be completed. This is done, after further regular refinements, which may be neccessary for structural reasons [31], by the green closures in figure 4. Irregular tetrahedra are never refined, instead all irregular refinements are skipped and the father tetrahedra are regular refined. For a more detailed description of the local refinement we refer to the literature mentioned above.

Before presenting numerical results for the adaptive FEM, we want to clarify the important question: What is the theoretical convergence we can expect at best? First, it is obvious that the FEM approximation, as well as the form of the adaptive refined

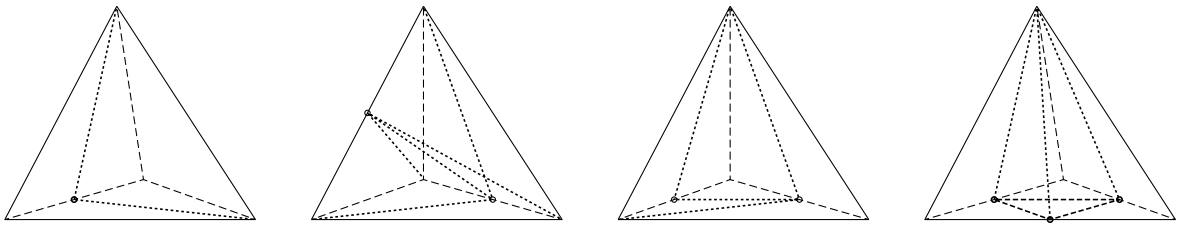

Figure 4 : Green closures

grid, depends on the polynomial approximation order p. In the case of an uniform triangulation, a non–degenerated eigenvalue and an eigenfunction of sufficient regularity, i.e. if Ψ is element of the Sobolew space H^{p+1}, a convergence behavior [32]

$$\delta E^{(p)} := |E - E^{(p)}| \leq C h^{2p} \tag{23}$$

for $h \to 0$ results. h denotes the typical gridsize and C a h–independent constant. For a 3D–domain Ω with typical size D, a uniform triangulation with N gridpoints leads to

$$h \approx \frac{D}{N^{1/3}} \tag{24}$$

and a convergence behavior

$$\delta E^{(p)}(N) = O(D^{2p}/N^{2p/3}) \quad . \tag{25}$$

can be achieved. In an h–adaptive method gridpoints are only added in regions, where they lead to an effective improvement of the FEM approximation, and the resulting mesh is not uniform. Thus a typical h–value in the sense of (24) is not well defined. But, the optimal mesh is characterized by equal local error contribution on each of the tetrahedra. Starting with an uniform grid this optimal triangulation can be obtained by a few adaptive refinement steps. A further improvement of the FEM solution leads to a refinement of all tedrahedra without changing the ratio of maximum to minimum grid size. For such (optimal) quasi–uniform grids a "typical" gridsize, for instance the average gridsize or the minimal gridsize, depends similar to (24) by

$$\bar{h} \approx \frac{D_{eff}}{N^{1/3}} \quad \text{with} \quad D_{eff} \leq D \tag{26}$$

on the number of gridpoints N. We come to a convergence behavior [33]

$$\delta E^{(p)}(N) = O(D_{eff}^{2p}/N^{2p/3}) \tag{27}$$

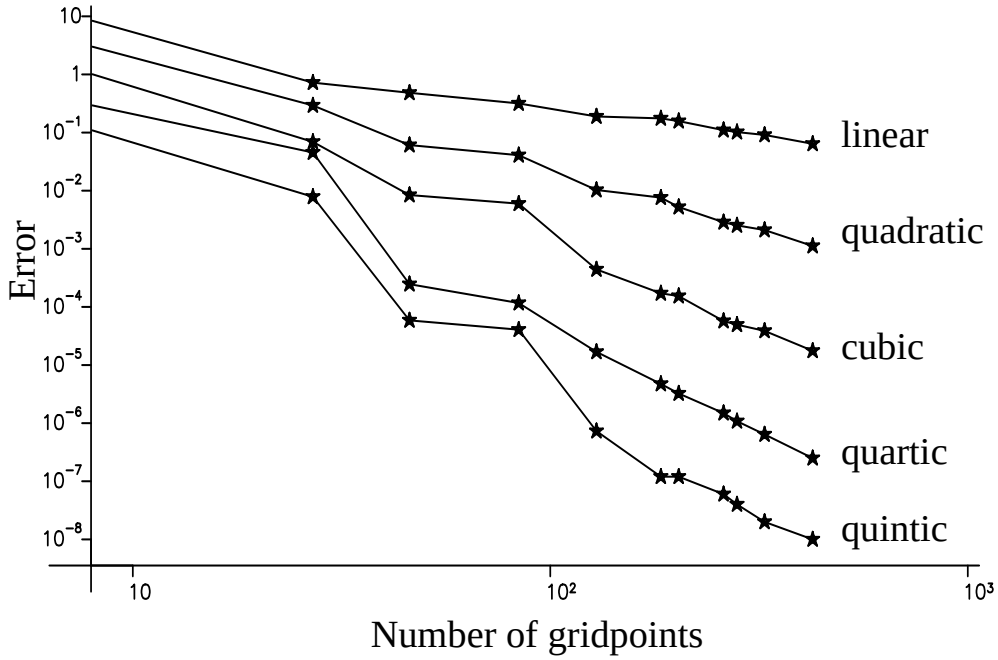

Figure 5 : Exact error for the eigenvalue of Hamiltonian (28) versus the number of gridpoints for polynomial order $p = 1, 2, 3, 4, 5$ (from above).

in the adaptive case. Ideally, both, the uniform refinement and the adaptive refinement, show a very similar asymptotic convergence behaviour. But, depending on the certain problem, the adaptive method can achieve a desired accuracy with much less gridpoints, i.e. with significantly less amount of computational work. This, in particular, will be the case for eigenvalue problems, where the domain Ω is very large, whereas the non–trivial part of the solution is located only in some small regions of Ω.

3. Numerical Results

A benchmark problem to test numerical methods for multidimensional eigenvalue equations is the vibrational motion of a mass in a three–dimensional non–isotropic harmonic potential. The Hamiltionian is given by (all quantities in the following given in atomar units)

$$\mathcal{H} = -\frac{1}{2}\vec{\nabla}^2 + k_x x^2 + k_y y^2 + k_z z^2 \tag{28}$$

in $L^2(\mathbb{R}^3, d^3x)$; force constants ($k_x = 0.5, k_y = 0.72, k_z = 0.845$) are set according to [34]. The wavefunction is approximated in the volume $\Omega := \{x, y, z \mid 0 \leq x, y, z \leq 6\}$, starting with an 8 point grid. A typical convergence behavior of the adaptive FEM approximation for the groundstate energy (exact value 1.75) with linear, quadratic, cubic, quartic and quintic polynomial order (solid lines from above, respectively) can be seen in figure 5. Here the exact error versus the number of gridpoints N is plotted in a "log–log" scale. For fixed p the approximation is improved by 11 adaptive refinements

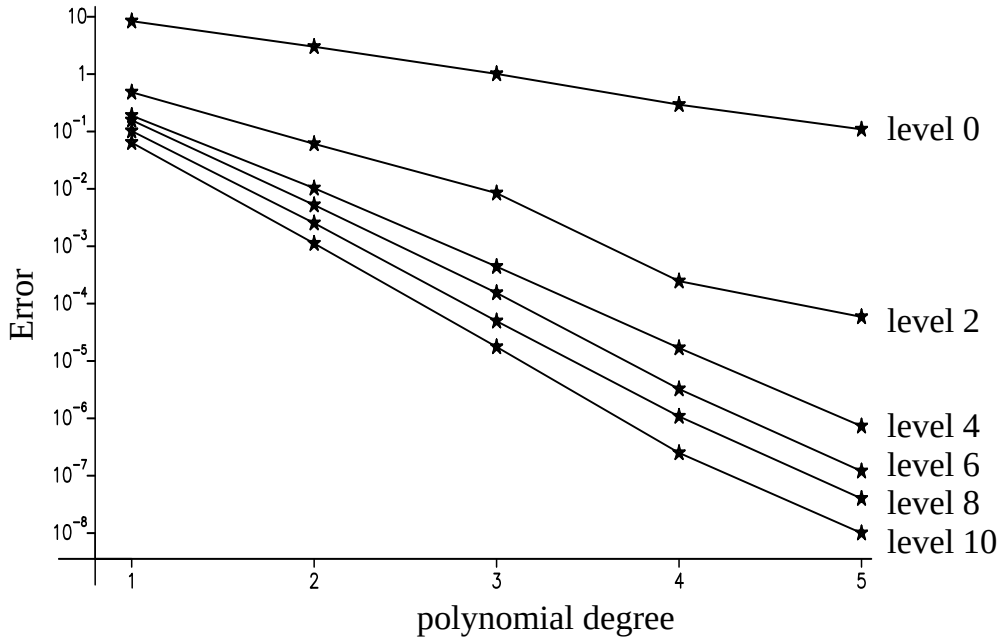

Figure 6 : Exact error of the eigenvalue for Hamiltonian (28) versus the polynomial aproximation order p at different refinement levels.

and for a fixed grid by increasing the polynomial order p from $p = 1$ up to $p = 5$. Following the exact errors along constant p values (solid lines) the asymptotic convergence behavior for $N \to \infty$ should be given by straight lines in this "log–log" plot if (27) is valid. Since we use an adaptive refinement based on the local errors (21) for $p = 4$ to obtain this particular result, only the exact error for the quartic approximation shows, after a few refinement levels, this optimal convergence behavior (27).

The exact error versus the local aproximation order p on different refinement levels is shown in a semi–logarithmic scale in figure 6. Again the optimal convergence behavior (27) would correspond to straight lines in this semilog plot. Since (27) is valid for uniform grids, this convergence behavior is given for the (uniform) initial grid. This behavior is destroyed by the local refinement (see level 2), but approximately again achieved for higher refinement levels, where the local errors are nearly equally distributed on the tetrahedra and the triangulation becomes quasi–uniform.

The estimation of the global error (19) plotted in figure 7 is always in the right scale and converges from below, see (20), to the exact error. The final precision in this computation reached with a 425 point grid ranges from $6 \cdot 10^{-2}$ for the linear approximation up to 10^{-8} for the quintic approximation. Of course the precision of the lower p approximation can be improved by further refinement steps, but the final precision is limited by the requirements on the cpu–time and the core of the computer being used (SUN Sparc 10). See therefore table 1, where we have used the error estimator for linear elements and pushed the final matrix dimension to values between 90000 and

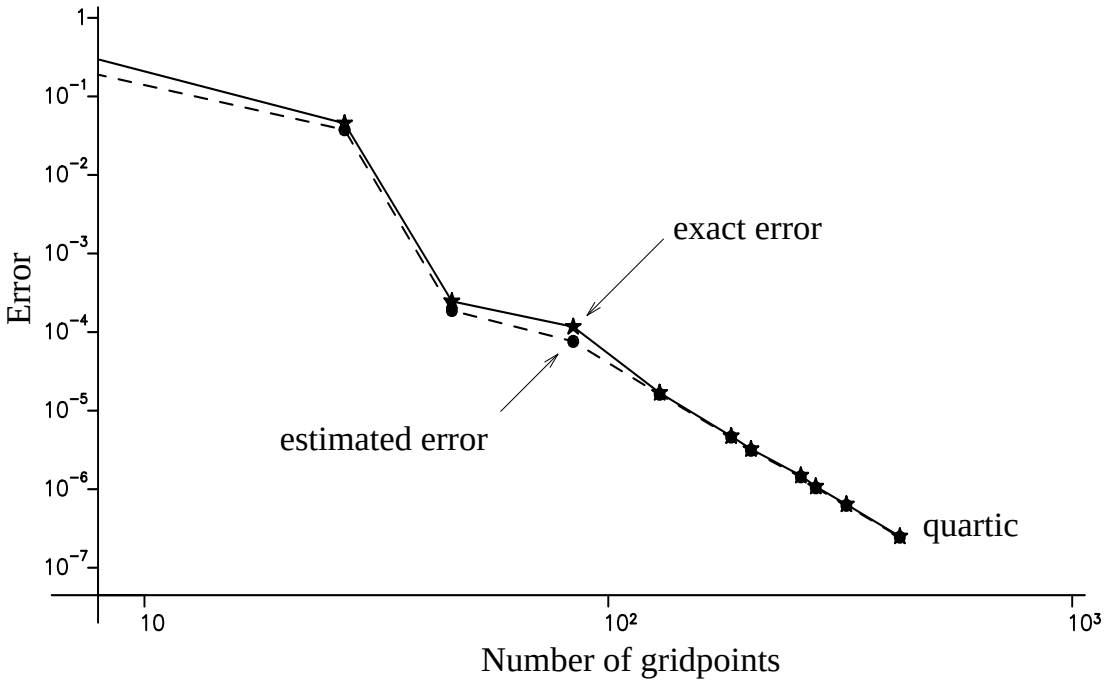

Figure 7 : Exact and estimated error for the adaptive FEM approximation of order $p = 4$ and Hamiltonian (28).

150000 for each p–value. Again the quintic approximation is superior to all lower order (but finer grid) approximations.

This example demonstrates, that the use of higher polynomial order shape functions is advantageous to obtain highly accurate results. But, a priori, this is not the case in FEM molecular structure calculations. Due to the nuclear cusps the wavefunction has no sufficient regularity ($\Psi \notin H^3(\mathbb{R}^3) \subset C^1(\mathbb{R}^3)$) to achieve a convergence behavior (27) for $p > 2$. On the other side it is well–known that such a reduction of the convergence order can be avoided if the singularity of the solution is isolated in a small tetrahedron [35]. To test the adaptive FEM for this kind of problems we use the quantum Hamiltonian for the adiabatic two–center one–electron problem in cartesian coordinates

$$\mathcal{H} = -\frac{1}{2}\nabla^2 - Z_1/ \mid \mathbf{r} - \mathbf{R} \mid - Z_2/ \mid \mathbf{r} \mid \tag{29}$$

for $Z_1 = Z_2 = 1$ (H_2^+ molecule) and $\mid \mathbf{R} \mid = 2.0$. The initial grid has 8 points, spanning the volume $\Omega := \{x, y, z \mid 0 \leq x, y, z \leq 10\}$. First, only the tetrahedra containing a nuclear center have been refined. These refinements towards the nuclear cusps is automatically repeated 12 times until the linear eigenvalue becomes stable (value -0.9883365). After 5 following adaptive refinements according to the local error estimator (21) for $p = 4$ the quintic energy -1.10263421 becomes accurate to 9 figures. The FEM eigenvalues obtained with the final 769 point mesh are listed in table 2.

After having demonstrated the applicability of the adaptive FEM to the treatment of the well–known H_2^+, we turn to a triatomic molecular system: the one–electron three–center problem. For simplicity we confine ourselves to the homonuclear D_{3h} symmetry

Table 1 :
FEM eigenvalues for the non–isotropic 3D harmonic oscillator (28).

shape function	M	energy	error
linear	92987	1.75112123	$1.1{\cdot}10^{-3}$
quadratic	152116	1.75000532	$5.3{\cdot}10^{-6}$
cubic	113325	1.75000045	$4.5{\cdot}10^{-7}$
quartic	95921	1.75000005	$5{\cdot}10^{-8}$
quintic	130326	1.75000000	$<1{\cdot}10^{-8}$
exact		1.75	

Table 2 :
Adaptive FEM results for the one–electron system H_2^+ at $R = 2.0$.

shape function	M	energy	error
linear	769	-1.05612693	$4.6{\cdot}10^{-2}$
quadratic	5230	-1.10177537	$8.6{\cdot}10^{-4}$
cubic	16730	-1.10262057	$1.4{\cdot}10^{-5}$
quartic	38615	-1.10263395	$2.6{\cdot}10^{-7}$
quintic	86501	-1.10263421	$<1{\cdot}10^{-8}$
exact		-1.10263421	

case, where the nuclear centers are located in a equilateral triangle geometry. The quantum Hamiltonian

$$\mathcal{H} = -\frac{1}{2}\nabla^2 - \ Z/\mid \mathbf{r}-\mathbf{R_1}\mid - Z/\mid \mathbf{r}-\mathbf{R_2}\mid - Z/\mid \mathbf{r}-\mathbf{R_3}\mid \tag{30}$$

with $\mid \mathbf{R_i}-\mathbf{R_{j\neq i}}\mid = R$, $i,j = 1,2,3$ describes for the physical value $Z = 1$ the equilateral H_3^{++}. It is of interest to study this Hamiltonian both from the theoretical and from the experimental point of view.

The isonuclear two–electron system for $Z = 1$, the H_3^+ molecule, stable in a equilateral triangle equilibrium geometry [39], may produce a (meta)stable H_3^{++} by photo–induced ionisation. Wether any state of H_3^{++} would enable this process is not known. Investigations [40] on the $^2A_1'$ groundstate, the $^2A_2''$ and E′ exited states of the D_{3h} ion indicate no local minima in the potential energy surfaces. But, whereas the H_3^+ ion, known from mass spectroscopy since 1912 [41] and playing an essential role in interstellar chemistry

Table 3 :
Results for the equilateral H_3^{+} at $R = 1.68$.

Ref.	function	M	energy	estimated error[a]
this work	linear	1051	-1.88929609e	$2.0{\cdot}10^{-2}$
this work	quadratic	7279	-1.90936535	$2.0{\cdot}10^{-4}$
this work	cubic	23448	-1.90956875	$2.2{\cdot}10^{-6}$
this work	quartic	54321	-1.90957096	$2.9{\cdot}10^{-8}$
this work	quintic	104661	-1.9095709876	—
Conroy [36]	STO		-1.9073	
Schwartz [37]	GTO		-1.90945	
Johnson *etal* [38]	GTO		-1.90945	
Johnson *etal* [38]	estimated exact		-1.9097	

[a] equation (19)

[42], has been studied over decades, the H_3^{2+} ion has not attracted too much interest from the computational chemistry. In fact, the accuracy of the electronic energy eigenvalues of the quantum Hamiltonian (30) we found in the literature [40, 43, 44, 38] are at best in the range of 10^{-4}. Note that benchmark calculations with 9 accurate figures have been reported [45] for the much more complicated two–electron ion H_3^{+}.

From a theoretical point of view, it is also of interest to investigate the Hamiltonian (30) for arbitary Z–values, as it has be done for diatomic systems [46–51,and literature therein]. A detailed knowledge of the binding metamorphosis of this system for varying Z may provide insights to universal effects, which occur in similar fashion in multiatomic systems with more electrons. A bridge to the mathematical physics may be possible by computing critical charge values separating the regime of stable, metastable and unstable binding. Based on rigorous theoretical results it is proven, that the homonuclear one–electron diatomic system in the Born–Oppenheimer approximation can have only monotonically decaying potential curves if Z$>$ 4 [52]. This is exactly the Z-value entailing the instability of the corresponding classical electrostatic system. The critical charge (Z = 1.5) for the instability of the classical triatomic system may play a similar role for the binding of the quantum three–center one–electron problem.

Since efforts in this direction are not the aim of this work we only present some benchmark calculations for this system, perhaps stimulating more detailed studies in the future. Calculation on different discretization domains have been performed with similar results, but different numerical requirements. The domain $\Omega := \{x, y, z \mid 0 \leq x \leq 10,\ x/\sqrt{3} \leq y \leq 10 - x/\sqrt{3},\ 0 \leq z \leq 10\}$ is appropriate to take advantage of the special D_{3h} symmetry; nuclear charges are located in the (x, y)–plane at

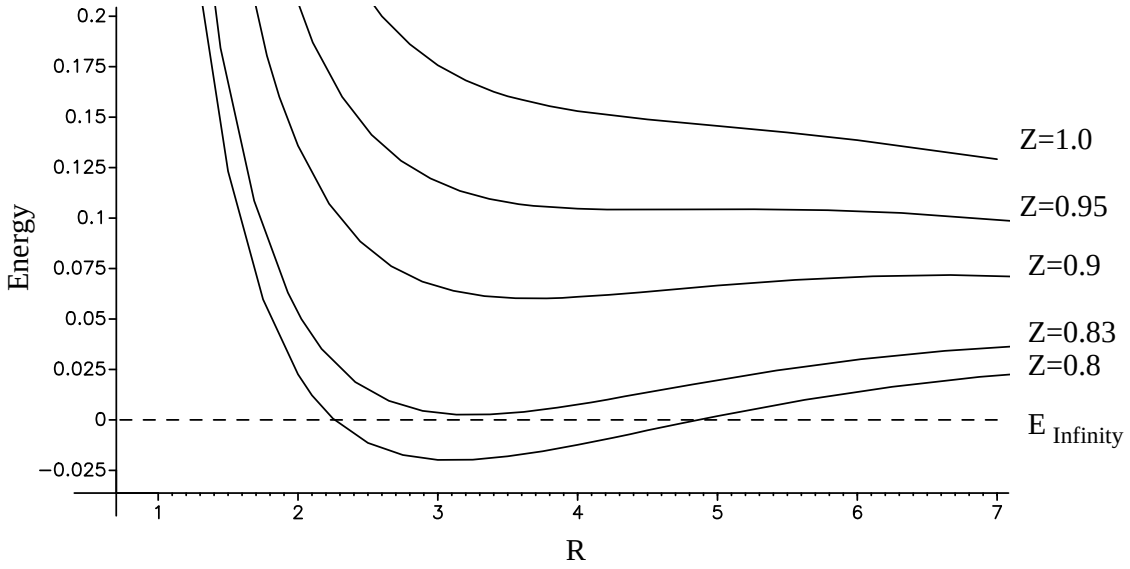

Figure 8: Total ground state energy curves (shifted by the asymptotic energy) for the equilateral one–electron three–center problem at different Z–values. R denotes the distance between two Coulomb centers.

$\mathbf{R_i} = (D\cos 2i\pi/3,\ D\sin 2i\pi/3,\ 0) \quad i = 1, 2, 3$, respectively, with $D = R/\sqrt{3}$. This domain is segmented into tetrahedra by the minimum number of 6 gridpoints for the initial mesh.

For a first benchmark calculation we select the internuclear distance $R = 1.68$. After 12 refinements towards the Coulomb singularities of the potential (30) the linear energy becomes stable (value -1.824026), indicating sufficient resolved cusps. Hence, by 7 adaptive refinements we get a 1051 point grid. The corresponding energy values for $p = 1 - 5$ are not affected for all indicated figures by further refinements towards the cusps. Obviously, the adaptive FEM energy values are of high accuracy and among the other theoretical data collected in table 3 most reliable. The quintic FEM eigenvalue -1.909 570 988 lowers the previous best upper bound energy by 1.2e-4 and lies about 1.e-4 above the estimated exact energy of Johnson and Poshusta [38]. The FEM discretization error, the so–called basis truncation error of the final quintic eigenvalue is approximately in the order of 4e-10. Increasing the accuracy of the gaussian integration formula from a 210 point formula (order 13) to a 495 point formula (order 17) [23] lowers the energy only by 5e-10. Thus the uncertainty of this value is mainly determined by the accuracy of the diagonalisation technique described in section 2. By this we assume an error in the order of 1.e-9 for the final quintic eigenvalue in table 3. For higher precision energies nonadiabatic as well as relativistic effects should be included.

Turning now to the stability question of the system for varying Z, energy values at about 35 different R-values in the range $0 < R \leq 7$ (for Z=1) have been calculated.

Varying Z in steps of $\Delta Z = 0.01$ in the range $0.8 < Z \leq 1.0$, the potential energy curves (total energy, including the nuclear-nuclear repulsion terms, versus R) enjoy a global minimum for $Z \leq 0.82$, while for $Z \geq 0.83$ this minimum has risen above the asymptotic energy. Increasing Z further, the depth of the local minimum drops to zero and vanishes finally at Z=0.96. Hence, the critical charges for stability are $Z_c^+ = 0.82 \pm 0.01$ and $Z_m^+ = 0.95 \pm 0.01$ for metastability, excluding in a definite manner any kind of stability of equilateral H_3^{++} in its groundstate.

4. Summary and outlook

The adaptive FEM turns out to be an efficient and rather universal tool for an accurate and error controlled treatment of the stationary Schrödinger equation in three space dimensions. For vibrational problems, as well as for molecular structure calculations the accuracy can be improved successively by the multilevel local refinement of the mesh. The final accuracy is limited only by the requirements on the cpu–time and the core of the computer beeing used. For the considered problems relative precisions better than 1e-8 are easily possible on a workstation.

Aside the three examples for which we obtained highly accurate results the program should be applicable to a rather broad range of relevant problems. For instance it would be worthwhile to test the adaptive FEM for the treatment of diabatic H_2^+ [15], for the approximation of correlated two–electron wavefunctions [4,53–56], for the study of the dynamical stability question of the H + e^+ system [50], for the vibrational motion of a mass in other three dimensional potentials, or for one–electron wavefunctions in other multi–center Coulomb systems.

An extension of the method to nonlinear systems, on the other hand, would enable very accurate basis free Hartree-Fock or density functional treatments for arbitrary multi electron systems.

References

[1] Ph.G. Ciarlet. *The Finite Element Method for Elliptic Problems*, volume 4 of *Studies in Mathematics and its Applications*. North Holland Publishing Company, Amsterdam, (1978).

[2] O. Axelsson and V.A. Barker. *Finite Element Solution of Boundary Value Problems*. Computer Science and Applied Mathematics. Academic Press, Inc., (1984).

[3] O.C. Zienkiewicz and R.L. Taylor. *The Finite Element Method*, volume 1. McGraw–Hill Book Company, London, 4 edition, (1989).

[4] José Luis Gáquez and Harris J. Silverstone. *J. Chem. Phys.* **67**, page 1887, (1977).

[5] P. Pyykkö, L. Laaksonen and D. Sundholm. *Int. J. Quantum Chem.* **23**, page 309, (1983).

[6] J.F. Flores. *J. Chem.Phys.* **98**, page 5642, (1983).

[7] W.K. Ford and F.S. Levin. *Phys. Rev. A* **29**, page 43, (1984).

[8] W. Schulze and D. Kolb. *Chem. Phys. Lett.* **122**, (1985).

[9] D. Heinemann, D. Kolb, and B. Fricke. *Chem. Phys. Lett.* **137**, page 180, (1987).

[10] B. Fricke D. Heinemann and D. Kolb. *Phys. Rev. A* **38**, page 4994, (1988).

[11] J. Shertzer. *Phys.Rev. A* **39**, page 3833, (1989).

[12] L. Yang, D. Heinemann, and D. Kolb. *Chem. Phys. Lett.* **178**, page 213, (1991).

[13] J.F. Flores. *Phys. Rev. A* **46**, page 6063, (1992).

[14] T.C. Scott, J. Shertzer, and R.A. Moore. *Phys. Rev. A* **45**,page 4393 (1992).

[15] J.F. Babb and J. Shertzer. *Chem. Phys. Lett.* **189**, page 287, (1992).

[16] L. Yang, D. Heinemann, and D. Kolb. *Phys. Rev. A* **49**, page 2700, (1993).

[17] J. Ackermann and R. Roitzsch. *Chem. Phys. Lett.* **214** , page 109, (1993).

[18] S. Hackel, D. Heinemann, D. Kolb, and B. Fricke. *Chem. Phys. Lett.* **206**, page 91, (1993).

[19] B. Erdmann, J. Lang and R. Roitzsch. KASKADE Manual. *Technical Report 93–5, Konrad–Zuse–Zentrum*, (1993).

[20] P. Deuflhard, P. Leinen, and H. Yserentant. *IMPACT Comput. Sci. Eng.* **1**, page 3, (1989).

[21] R.E. Bank. *PLTMG — a software package for solving elliptic partial differential equations, user's guide 6.0.SIAM.* Philadelphia, (1990).

[22] A.H. Stroud. *Approximate Calculation of Multiple Integrals.* Prentice–Hall,Inc.,Englewood Cliffs, New Jersey, (1971).

[23] A. Grundmann and H.M. Möller. *SIAM J. Num. Anal.* **15**, page 282, (1978).

[24] A. George and J.W.-H. Liu. *Computer Solution of Large Sparse Positive Definite Systems.* Pretice–Hall,Inc.,Englewood Cliffs, New Jersey, (1981).

[25] F. Bornemann, B. Erdmann, and R. Kornhuber. Preprint SC 93–29, Konrad–Zuse–Zentrum, Berlin, (1993).

[26] R.E. Bank, A.H. Sherman, and H. Weiser. Refinement algorithms and data structures for regular local mesh refinement. In R. Stepleman et at, editor, *Scientific Computing*, pages 3–17. North–Holland, Amsterdam, (1983).

[27] S. Zhang. PhD thesis, Pennsylvania State University, Pennsylvania, (1988).

[28] M. E. Go Ong. PhD thesis, University of California, Los Angeles, (1989).

[29] J. Bey. Master's thesis, RWTH Aachen, 1991.

[30] E. Bänsch. *IMPACT Comp. Sci. Eng.* **3**, page 181, (1991).

[31] F. Bornemann, B. Erdmann, and R. Kornhuber. *Int. J. for Num. Meth. in Eng.* **36**, page 3187, (1993).

[32] W. Hackbusch. *Theorie und Numerik elliptischer Differentialgleichungen.* B.G. Taubner Stuttgart, 1986.

[33] I. Babuška and B. Szabó. *Int. J. for Num. Meth. in Eng.* **18**, page 323, (1982).

[34] RJ.R. Alvarez-Collado and R.J. Buenker. *J. Comp. Chem.***13**, pages 135–141, (1992).

[35] Z.H. Levine and J.W. Wilkins. *J. Comp. Phys.* **83**, page 361, (1989).

[36] H. Conroy. *J. Chem. Phys.* **41**, page 1327, (1964).

[37] M.E. Schwartz. PhD thesis, Vanderbilt University, Nashville, Tenn., (1966).

[38] J.W. Johnson and R.D. Poshusta. *Int. J. Quantum Chem.* **11**, page 885, (1977).

[39] W. Meyer, P. Botschwina, and P. Burton. *J. Chem. Phys.* **84**, page 891, (1986).

[40] H. Conroy. *J. Chem. Phys.* **51**, page 3979, (1969).

[41] J.J. Thomson. *Philos. Mag.* **24**, page 209, (1912).

[42] T. Oka. *Rev. Mod. Phys.* **64**, page 1141, (1992).

[43] R.M. Shoucri and B. T. Darling. *J. Chem. Phys.* **56**, page 1789, (1972).

[44] J.A. Hernádez and R. Carbó. *J. Chem. Phys.* **62**, page 2637, (1975).

[45] R. Röhse and W. Klopper and W. Kutzelnigg. *J. Chem. Phys.* **99**, page 8830, (1993).

[46] G.A. Arteca and P.G. Mezey. *Phys. Rev.* **35**, page 4044, (1987).

[47] J. Ackermann and K. Helfrich. *Z. Phys. D* **18**, page 365, (1991).

[48] J. Ackermann and H. Hogreve. *J. Phys. B* **25**, page 4069, (1992).

[49] B.L.Laurenzi and D.R. Gaylord. *Int. J. Quantum Chem.* **44**, page 17, (1992).

[50] H. Hogreve. *J. Chem. Phys.* **98**, page 5579, (1993).

[51] H. Hogreve. *Phys. Rev. A* **48**, page 3382, (1993).

[52] P. Duclos and H. Hogreve. In J. Dittrich and P. Exner, editors, *Proc. Conf. in Rigorous Results in Quantum Dynamics (Liblice 1990)*, page 63, (1991).

[53] N.W. Winter, A. Laferrière, and V. McKoy. *Phys. Rev. A* **2**, page 49, (1970).

[54] I.L. Hawk and D.L. Hardcastle. *Computer Physics Communications* **16**, page 159, (1979).

[55] F.S. Levin and J. Shertzer. *Phys. Rev. A* **32**, page 3285, (1985).

[56] C. Bottcher, D.R. Schulz, and D.H. Madison. *Phys. Rev. A* **49**, page 1714, (1994).